SCIENCE CHINA
Physics, Mechanics & Astronomy

• Article •

October 2021 Vol. 64 No. 10: 107211
https://doi.org/10.1007/s11433-021-1750-2

Optical detection of quantum geometric tensor in intrinsic semiconductors

Zhi Li[1*], Shengli Zhang[1], Takami Tohyama[2], Xiufeng Song[1], Yu Gu[1], Toshiaki Iitaka[3], Haibin Su[4], and Haibo Zeng[1*]

[1] *MIIT Key Laboratory of Advanced Display Materials and Devices, Ministry of Industry and Information Technology, Institute of Optoelectronics & Nanomaterials, Nanjing University of Science and Technology, Nanjing 210094, China;*
[2] *Department of Applied Physics, Tokyo University of Science, Katsushika, Tokyo 125-8585, Japan;*
[3] *Discrete Event Simulation Research Team, RIKEN Center for Computational Science, Wako 351-0198, Japan;*
[4] *Department of Chemistry, The Hong Kong University of Science and Technology, Hong Kong, China*

Received May 18, 2021; accepted July 22, 2021; published online September 2, 2021

Quantum geometric tensor, including a symmetric real part defined as quantum metric and an antisymmetric part defined as Berry curvature, is essential for understanding many phenomena. In this study, we investigated the photogalvanic effect of semiconductors with time-reversal-invariant and spatial inversion symmetries using the quantum kinetic equation. We concluded that the integral of the symmetric (antisymmetric) part of quantum geometric tensor on the equal energy surface in momentum space, satisfying the resonance condition, is related to the generation rate of carriers in semiconductors under linearly (circularly) polarized light. Under additional bias voltage, the dc photocurrent is proportional to the bias voltage. Our study provided an alternative interpretation for the photogalvanic effect in the view of quantum geometric tensor. Additionally, it classified the intrinsic difference between linearly and circularly polarized optical fields.

quantum geometry, photovoltaic effect, nonlinear optics

PACS number(s): 04.60.Pp, 72.40.+w, 42.65.-k

Citation: Z. Li, S. Zhang, T. Tohyama, X. Song, Y. Gu, T. Iitaka, H. Su, and H. Zeng, Optical detection of quantum geometric tensor in intrinsic semiconductors, Sci. China-Phys. Mech. Astron. **64**, 107211 (2021), https://doi.org/10.1007/s11433-021-1750-2

1 Introduction

Geometry plays a significant role in various aspects of modern physics [1-4]. The geometry of the eigenstates is encoded in the quantum geometric tensor (QGT) [5-9] defined on any manifold of states smoothly varying with some parameter λ. The geometric tensor naturally appears when one defines the "distance" between nearby states $|\psi(\lambda)\rangle$ and $|\psi(\lambda + \mathrm{d}\lambda)\rangle$.

$$\mathrm{d}s^2 = 1 - |\langle\psi(\lambda)|\psi(\lambda + \mathrm{d}\lambda)\rangle|^2 = \mathrm{d}\lambda_\alpha Q_{\alpha\beta}\mathrm{d}\lambda_\beta + O(|\mathrm{d}\lambda|^3), \quad (1)$$

where $Q_{\alpha\beta} = \Gamma_{\alpha\beta} + \mathrm{i}\Omega_{\alpha\beta}$ is an object known as the geometric tensor consisting of antisymmetric Berry curvature $\Omega_{\alpha\beta}$ and symmetric quantum metric $\Gamma_{\alpha\beta}$. The Berry curvature is essential for topological matter [10-16], and the quantum metric defines the distance between eigenstates. The knowledge of the quantum metric is essential for understanding several

*Corresponding authors (Zhi Li, email: zhili@njust.edu.cn; Haibo Zeng, email: zeng.haibo@njust.edu.cn)

phenomena, such as the orbital magnetic susceptibility [17], exciton Lamb shift [18], and anomalous Hall drift [19].

Nonlinear optical response [20], including the second harmonic generation (SHG) and photogalvanic effect (PGE), has wide applications in the scientific community [21]. For example, SHG is used for frequency doubling of laser light and the detection of the breaking of spatial inversion symmetry (SIS) [22]. The PGE, where the dc electronic current is induced when the material is illuminated by light, can occur in materials with broken SIS without bias [23-28]. There are two types of PGE in semiconductors: injection and shift currents. The injection current is also called circular PGE (CPGE) since the direction of current is determined by the helicity of light. CPGE can be used for detecting the topological charge of quantum matter [29-35], i.e., CPGE is related to the Berry curvature. The direction of shift current is independent of the helicity of light; hence this is also known as linear PGE (LPGE). For materials with SIS, if no dc bias voltage is applied to drive the carrier pumped by light, both CPGE and LPGE vanish. Recently, the Berry curvature dipole (BCD) defined as the integral of the gradient of the Berry curvature in momentum space [36-40] offers a new mechanism for PGE in metallic materials. Bilayer WTe_2 with a tilted Weyl point provides a possible platform for detecting the BCD and its induced nonlinear Hall current [41-45]. Since the CPGE is related to the antisymmetric Berry curvature of occupied states, we probably wonder what the role of the symmetric quantum metric is. If we can connect the symmetric quantum metric to some nonlinear optic effect, we can bridge the gap between the nonlinear optical effect and QGT.

In this study, we addressed the basic theory of PGE of intrinsic semiconductors with TRIS and SIS under an applied dc bias voltage. We observed that the integral of the symmetric (antisymmetric) part of QGT on the equal energy surface in momentum space satisfying the resonance condition is related to the generation rate of carriers in semiconductors under linearly (circularly) polarized light with photon energy larger than the bandgap. Under additional bias voltage, the driven photocurrent is proportional to the bias voltage. Our study builds close connections between the nonlinear optical response of the system using TRIS and QGT of quantum states. It clarifies the underlying cause of the tensor field for the nonlinear optical response. Additionally, our study facilitates the detection of a QGT using photocurrent measurement.

2 Quantum kinetic equation

We consider a typical experimental setup of a biased photoconductor under irradiation (Figure 1). The pump light hits the surface of the semiconductor material with TRIS and SIS. The bias voltage is applied along the z-direction to drive the carrier pumped by the laser light. Under spatial homogeneous optical field $\mathbf{E}(t) = \mathbf{E}(\omega)e^{-i\omega t} + c.c.$, light-matter interaction can be described by the following model Hamiltonian in length gauge,

$$H(t) = \int d^3\mathbf{r}\Psi^{\dagger}(\mathbf{r},t)[H_0 - e\mathbf{E}(t)\cdot\mathbf{r}]\Psi(\mathbf{r},t), \tag{2}$$

where H_0 is the unperturbed single-particle Hamiltonian, and $H_1 = -e\mathbf{E}(t)\cdot\mathbf{r}$ describes the light-matter interaction. The strength of the electric field $\mathbf{E}$(t) can include the static component, which plays the role of bias voltage. Although the light-matter interaction has another description in the velocity gauge, we have adopted the length gauge because of unphysical divergences that arise in the velocity gauge [46,47]. The orthogonal Bloch functions $\phi_n(\mathbf{k},\mathbf{r})$ satisfy

$$H_0\phi_n(\mathbf{k},\mathbf{r}) = \epsilon_n(\mathbf{k})\phi_n(\mathbf{k},\mathbf{r}), \tag{3}$$

where n is the band index, and $\mathbf{k}$ is position vector in momentum space. The Bloch functions are orthogonal to each other,

$$\int d^3\mathbf{r}\phi_n^{\dagger}(\mathbf{k},\mathbf{r})\phi_m(\mathbf{k}',\mathbf{r}) = \delta_{nm}\delta(\mathbf{k}-\mathbf{k}'). \tag{4}$$

The wave function $\Psi(\mathbf{r},t)$ can be expressed as a combination of Bloch functions with coefficients $a_n(\mathbf{k},t)$,

$$\begin{aligned}\Psi(\mathbf{r},t) &= \sum_n \int_{\mathrm{BZ}} \frac{d^3\mathbf{k}}{(2\pi)^3} a_n(\mathbf{k},t)\phi_n(\mathbf{k},\mathbf{r}) \\ &= \sum_{n,\mathbf{k}} a_n(\mathbf{k},t)\phi_n(\mathbf{k},\mathbf{r}).\end{aligned} \tag{5}$$

The dynamics of the density operator $\rho(t) = |\Psi(t)\rangle\langle\Psi(t)|$ can be described using the quantum kinetic equation with constant relaxation time [48-51],

$$i\hbar\frac{\partial\rho(t)}{\partial t} = [H,\rho(t)] + i\hbar\frac{\delta\rho(t)}{\tau}, \tag{6}$$

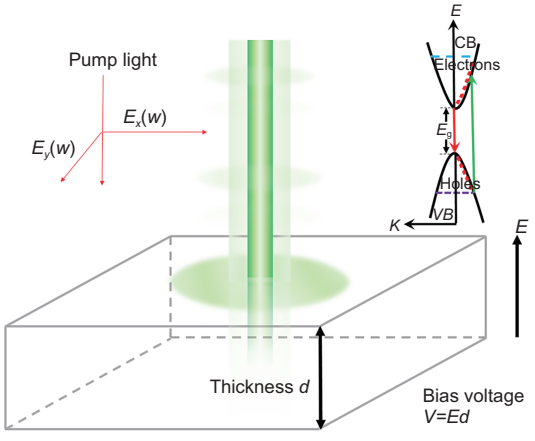

Figure 1 (Color online) Schematic diagram for the experimental setup.

where τ is the relaxation time. We expand the density matrix to second-order field strength,

$$\rho_{nm}(\mathbf{k},t)=\rho^{(0)}_{nm}(\mathbf{k})+\rho^{(1)}_{nm}(\mathbf{k},t)+\rho^{(2)}_{nm}(\mathbf{k},t), \tag{7}$$

where $\rho_{nm}(\mathbf{k},t)=\langle n(\mathbf{k})|\rho|m(\mathbf{k})\rangle$. From eq. (6), the first-order inter-band ($n\neq m$) density matrix is given as follows:

$$\rho^{(1)}_{nm}(\mathbf{k},\omega)=\frac{\langle n|H_1(\omega)|m\rangle(\rho^{(0)}_{mm}(\mathbf{k})-\rho^{(0)}_{nn}(\mathbf{k}))}{\hbar\omega-\epsilon_{nm}(\mathbf{k})-\mathrm{i}\eta}, \tag{8}$$

where $\epsilon_{nm}(\mathbf{k})=\epsilon_n(\mathbf{k})-\epsilon_m(\mathbf{k})$. The intra-band first-order density matrix is given as follows:

$$\rho^{(1)}_{nn}(\mathbf{k},\omega)=\frac{-\mathrm{i}e}{\hbar\omega-\mathrm{i}\eta}\mathbf{E}(\omega)\cdot\partial_{\mathbf{k}}\rho^{(0)}_{nn}(\mathbf{k}). \tag{9}$$

Here, $\rho^{(0)}_{nn}(\mathbf{k})=\frac{1}{1+\exp(\frac{\epsilon_n(\mathbf{k})-\mu}{k_BT})}$ (k_B Boltzmann constant, T temperature, μ chemical potential) is Fermi-Dirac distribution of band n, and $\eta=\hbar/\tau$. For intrinsic semiconductor, the intra-band first-order density matrix $\rho^{(1)}_{nn}(\mathbf{k},\omega)$ vanishes completely. For linear response, the ac current along y-direction is given as follows:

$$J_y(\omega)=\frac{e}{(2\pi)^3}\sum_{nm}\int \mathrm{d}^3k\left\langle m(\mathbf{k})\left|\frac{\partial H_0(\mathbf{k})}{\hbar\partial k_y}\right|n(\mathbf{k})\right\rangle\rho^{(1)}_{nm}(\mathbf{k},\omega). \tag{10}$$

In the limit of low frequency and clean system, viz, relaxation time is infinite, photon energy $\hbar\omega$ is smaller than the bandgap E_g, and $\eta\sim 0$. The imaginary part of the optical conductivity is given by

$$\sigma_{yx}(\omega)=\frac{\mathrm{i}e^2\omega}{(2\pi)^3}\sum_{nm}\int \mathrm{d}^3k\frac{\Gamma^{xy}_{nm}(\mathbf{k})}{\epsilon_{nm}(\mathbf{k})}\rho^{(0)}_{mm}(\mathbf{k}), \tag{11}$$

where, the inter-band metric tensor $\Gamma^{xy}_{nm}(\mathbf{k})$ is given by

$$\begin{aligned}2\Gamma^{xy}_{nm}(\mathbf{k})=&\langle\partial_x m(\mathbf{k})|n(\mathbf{k})\rangle\langle n(\mathbf{k})|\partial_y m(\mathbf{k})\rangle\\&+\langle\partial_y m(\mathbf{k})|n(\mathbf{k})\rangle\langle n(\mathbf{k})|\partial_x m(\mathbf{k})\rangle.\end{aligned} \tag{12}$$

The real part of the optical conductivity describes the quantum Hall effect, and it should vanish for topologically trivial semiconductors. For resonance, the real part of the optic conductivity is given by

$$\sigma_{yx}=\frac{-\pi e^2}{\hbar(2\pi)^3}\oint 2\Gamma^{xy}_{cv}(\mathbf{k}). \tag{13}$$

The integral should be calculated on an equal energy surface in momentum space satisfying $\hbar\omega=E_g$. If there is multiple pair of the conduction band (c) and valence band (v) satisfying $\hbar\omega=E_g$, we should sum contributions from all pairs. Thus, we classify the role of the metric tensor in the linear response.

From eq. (6), the second-order intra-band density matrix is given as follows:

$$\mathrm{i}\hbar\frac{\mathrm{d}\rho^{(2)}_{cc}(\mathbf{k},t)}{dt}=\langle c|[H_1,\rho^{(1)}]|c\rangle+\mathrm{i}\hbar\frac{\rho^{(2)}_{cc}(\mathbf{k},t)}{\tau}, \tag{14}$$

where $|c(\mathbf{k})\rangle$ is the Bloch state of a conduction band. The intra-band photocurrent, including injection and anomalous currents induced by BCD, vanishes in semiconductors with SIS and TRIS. However, the density of carriers is not vanishing. After some straightforward calculations as shown in Supporting Information, the density of conducting electron with zero frequency is given by

$$n_c=\int\frac{\mathrm{d}\mathbf{k}}{(2\pi)^3}\rho^{(2)}_{cc}(\mathbf{k})=G\tau, \tag{15}$$

where G is the generation rate of carriers with zero frequency. For linearly polarized optical field applied in xy-plane, the carrier generation rate is given by

$$G(\omega)=(4\pi)^2\alpha P\int\frac{\mathrm{d}\mathbf{k}}{(2\pi)^3}\Gamma_{xy}(\mathbf{k})\delta(\hbar\omega-\epsilon_{cv}(\mathbf{k})), \tag{16}$$

where the fine structure constant $\alpha=\frac{e^2}{4\pi\hbar c\varepsilon_0}$, and power density $\mathrm{P}=\frac{1}{2}c\varepsilon_0|E|^2$. This equation demonstrates that the carrier generation rate is proportional to the power density. Further, it connects the generation rate with the symmetric quantum metric tensor $\Gamma_{xy}(\mathbf{k})$. If the low energy dispersion near the Fermi level can be described via a pair of conduction and valence bands, the quantum metric tensor of band c is given by

$$\begin{aligned}\Gamma_{xy}(\mathbf{k})=&\frac{1}{2}\langle\partial_x c|\partial_y c\rangle+\frac{1}{2}\langle\partial_y c|\partial_x c\rangle\\&+\frac{1}{2}\langle c|\partial_x c\rangle\langle c|\partial_y c\rangle+\frac{1}{2}\langle c|\partial_y c\rangle\langle c|\partial_x c\rangle,\end{aligned} \tag{17}$$

where ∂_x means $\frac{\partial}{\partial k_x}$. This tensor is symmetric under the exchange of x and y. It is a function of momentum $\mathbf{k}$, viz, this quantum metric tensor is non-vanishing even though TRIS and SIS are preserved. For multiple-band systems, we should sum contribution from all pairs of band satisfying $\hbar\omega=E_g$, and the metric tensor should be defined as eq. (12).

Under circularly polarized optical field applied in xy-plane, the generation rate of carrier is given as:

$$G=(4\pi)^2\alpha P\int\frac{\mathrm{d}\mathbf{k}}{(2\pi)^3}\Omega_{xy}(\mathbf{k})\delta(\hbar\omega-\epsilon_{cv}(\mathbf{k})), \tag{18}$$

where $\Omega_{xy}(\mathbf{k})=\mathrm{i}\langle\partial_x c|\partial_y c\rangle-\mathrm{i}\langle\partial_y c|\partial_x c\rangle+\mathrm{i}\langle c|\partial_x c\rangle\langle c|\partial_y c\rangle-\mathrm{i}\langle c|\partial_y c\rangle\langle c|\partial_x c\rangle$ is the Berry curvature defined in momentum space for two-band model systems. In contrast to quantum metric tensor, this curvature tensor is zero in materials with TRIS and SIS. However, the Berry curvature is nonzero in topological materials with broken SIS or TRIS. Both CPGE

and nonlinear Hall effect are related to the Berry curvature. The inter-band density is given as:

$$\rho^{(2)}_{nm}(\mathbf{k},\omega_3)=\sum_{\omega_1,\omega_2}\frac{e\mathbf{E}(\omega_1)\cdot\mathbf{D}_{nm}(\mathbf{k})}{\hbar\omega_3-\epsilon_{nm}(\mathbf{k})}\rho^{(1)}_{nm}(\omega_2)\times\delta(\omega_3,\omega_1+\omega_2).$$

Here, the shift vector $\mathbf{D}_{nm}$ is defined as $\mathbf{D}_{nm}(\mathbf{k})=-\mathrm{i}\partial_{\mathbf{k}}+\mathbf{A}_{mm}(\mathbf{k})-\mathbf{A}_{nn}(\mathbf{k})$, and $\mathbf{A}_{mm}(\mathbf{k})=\mathrm{i}\langle c|\partial_{\mathbf{k}}c\rangle$ is the Berry connection [52]. The shift vector $\mathbf{D}_{nm}$ is invariant under the gauge transformation of Bloch functions. It characterizes the difference between intracell position matrices within the valence and conduction bands. Additionally, it underlies the shift current in non-centrosymmetric semiconductors. For semiconductors with both TRIS and spatial inversion invariant symmetry, we can adopt a proper local phase gauge for Bloch function to make Berry connection vanish over the entire BZ; however, it may be impossible in materials with broken SIS. Since $\rho^{(1)}_{nm}(\mathbf{k},\omega)$ is an even function of momentum $\mathbf{k}$, the integral of inter-band matrix element $\rho^{(2)}_{nm}(\omega_3)$ in momentum space is vanishing. For semiconductors with broken SIS, the inter-band dc current (shift current) contribution is not vanishing.

3 Application to massive Dirac model Hamiltonian

For applied optical field (pump light) with a frequency larger than the bandgap E_{g}, all electrons with momentum $\hbar\omega=\epsilon_{cv}(\mathbf{k})$ can be excited, and the domain of integration is same as the energy surface in momentum space. If the frequency of the optical field is same as the bandgap of the direct gap semiconductor, only the electron at the topmost point of the valence band can be excited. The domain of integration is reduced to discrete momentum points satisfying $\hbar\omega=E_{\mathrm{g}}$. Therefore, the dc bias voltage is not responsible for producing carriers, whereas it only accelerates the carriers. To clarify the physical meaning of quantum metric and estimate its magnitude, we take the halide perovskite $CsPbBr_3$ as an example. Cubic $CsPbBr_3$ is a direct bandgap semiconductor with E_{g}=2.43 eV at Γ=(0,0,0) point. The band dispersion near Γ point can be described as the low energy effective Hamiltonian,

$$H_0(\mathbf{k})=\begin{pmatrix}\Delta & V(\mathbf{k})\\ V^{\dagger}(\mathbf{k}) & -\Delta\end{pmatrix},\tag{19}$$

where the off-diagonal term $V(\mathbf{k})$ describing orbital hybridization, including the spin-orbital coupling, is given as:

$$V(\mathbf{k})=\begin{pmatrix}\gamma_z k_z & \gamma_x k_x-\mathrm{i}\gamma_y k_y\\ \gamma_x k_x+\mathrm{i}\gamma_y k_y & -\gamma_z k_z\end{pmatrix},\tag{20}$$

where the positive 2Δ is the charge transfer energy between the s-orbital of cation and p-orbital of halogen ions, and $\gamma=(\gamma_x,\gamma_y,\gamma_z)$ is a set of parameters tuning the anisotropic strength of orbital hybridization $V(\mathbf{k})$ with spin-orbital coupling. Since the valence and conduction bands near the Fermi level are dominated by the s-orbitals from cation and p-orbitals from halogen, respectively, the hybridization term should be an odd function of momentum $\mathbf{k}$. We neglect higher order off-diagonal elements $\propto k^3$. From the unperturbed Hamiltonian $H_0(\mathbf{k})$ in eq. (14), the four band dispersions are given as follows:

$$\epsilon_{v_\uparrow}(\mathbf{k})=\epsilon_{v_\downarrow}(\mathbf{k})=-d(\mathbf{k}),$$
$$\epsilon_{c_\uparrow}(\mathbf{k})=\epsilon_{c_\downarrow}(\mathbf{k})=d(\mathbf{k}),$$
$$d(\mathbf{k})=\sqrt{\Delta^2+[(\gamma_x k_x)^2+(\gamma_y k_y)^2+(\gamma_z k_z)^2]}.$$

However, the periodic part of the Bloch function is given by

$$|v_\uparrow(\mathbf{k})\rangle=\eta(\,\gamma_z k_z\quad\gamma_x k_x+\mathrm{i}\gamma_y k_y\quad-(d+\Delta)\quad 0\,)^{\mathrm{T}},$$
$$|v_\downarrow(\mathbf{k})\rangle=\eta(\,\gamma_x k_x-\mathrm{i}\gamma_y k_y\quad-\gamma_z k_z\quad 0\quad-(d+\Delta)\,)^{\mathrm{T}},$$
$$|c_\uparrow(\mathbf{k})\rangle=\eta(\,d+\Delta\quad 0\quad\gamma_z k_z\quad\gamma_x k_x+\mathrm{i}\gamma_y k_y\,)^{\mathrm{T}},$$
$$|c_\downarrow(\mathbf{k})\rangle=\eta(\,0\quad d+\Delta\quad\gamma_x k_x-\mathrm{i}\gamma_y k_y\quad-\gamma_z k_z\,)^{\mathrm{T}},$$

where $\eta=\frac{1}{\sqrt{2d(d+\Delta)}}$. Both band dispersions and wavefunctions are differentiable over the entire BZ. For the ground state, the electronic distribution on different bands obeys the Fermi-Dirac distribution approximately, neglecting the temperature dependence because of the large bandgap in $CsPbBr_3$. $H_0(\mathbf{k})$ is the massive Dirac Hamiltonian [53, 54], describing the linear band dispersion of massive Dirac fermion with mass Δ. At Γ point, the quantum metric $\Gamma_{xx}(0,0,0)=\gamma_x^2/E_{\mathrm{g}}^2$, $\Gamma_{yy}(0,0,0)=\gamma_y^2/E_{\mathrm{g}}^2$, and $\Gamma_{xy}(0,0,0)=0$. This result shows that quantum metric strongly depends on the bandwidth and bandgap determined by the bond strength and charge transfer energy, respectively. The enhancement of bond strength and reduction of charge transfer energy can significantly increase the magnitude of the quantum metric. For $\gamma_x=\gamma_y=\hbar v_{\mathrm{F}}=2.43$ eV·Å, i.e., inter-band electronic velocity $v_{\mathrm{F}}=2.43\times10^5$ m/s, the estimated $\Gamma_{xx}=\Gamma_{yy}\sim1$ Å^2. Under optical field with photon energy $\hbar\omega=E_{\mathrm{g}}+0^+$, the integral domain is reduced to spherical surface surrounding the Γ point, and the generation rate is given by

$$G(\omega)=8\alpha P\Gamma_{xx}(\mathbf{k}=0)/E_{\mathrm{g}}.\tag{21}$$

For power density $P=3.88$ mW/cm^2, the generation rate is $\frac{8}{137}$ s^{-1}. With typical duration of laser light $\tau=1$ ps and valence electron density $N=2\times10^{24}$/cm^3, the static conducting electron density $n_c=16/137\times10^{12}$/cm^3. The average electron-electron distance is about 200 μm. We neglect the

electron-electron collision or correlation because of the low carrier density. Additionally, if it is possible to extract the carrier generation rate information from the experiment, we can estimate the quantum metric of the direct gap semiconductor using this equation.

Although the finite density of carriers can be produced using light with photon energy larger than bandgap, dc current is still absent in semiconductors with TRIS and SIS. However, we can drive the carriers to form dc current through static bias voltage. The drift velocity of carriers induced by bias electric field along z-direction is $v = -e\tau E_{\rm b}\frac{m_{\rm e}+m_{\rm h}}{m_{\rm e}m_{\rm h}}$, where $m_{\rm e}$ ($m_{\rm h}$) is the effective mass of electron (hole). The current density is given by

$$j_z = -NG\tau v = -(e\tau)^2 NGE_{\rm b}\frac{m_{\rm e}+m_{\rm h}}{m_{\rm e}m_{\rm h}}. \tag{22}$$

With typical parameters τ=1 ps [55], the density of valence electron is $N = 2\times10^{24}/{\rm cm}^3$, $m_{\rm e} = m_{\rm h} = 0.2m_0$ (m_0 is the mass of electron), small bias electric field is $E_{\rm b} = 0.1$ V/cm, which is about 1/10 strength of the oscillating optical field, and the estimated current density is about 3.3 nA/cm^2. This photocurrent is proportional to the bias voltage, and it will vanish under circularly polarized light. It is worth noting that the tetragonal phase of $CsPbBr_3$ is non-centrosymmetric, and the low energy band dispersion can be described by a pair of massive Weyl fermions with opposite chirality instead of massive Dirac fermion. Thus, CPGE is possible in the tetragonal phase [56, 57].

Finally, we discuss the recent measurement of photocurrent in palladium ditelluride ($PdTe_2$) under Terahertz [58]. The bulk $PdTe_2$ single crystal has a space group $P\bar{3}m1$, and it is centrosymmetric. The low energy band dispersion can be described by a massless Dirac electron. Under zero bias voltage, the photocurrent is not completely vanishing in some $PdTe_2$-based devices due to the symmetry of electrodes. Although the bulk $PdTe_2$ is metallic, the photocurrent is still approximately proportional to the bias voltage and vanishes under circularly polarized light.

4 Summary

In summary, motivated by the CPGE observed in topological matters, we addressed the basic theory of PGE of materials with TRIS and spatial inversion symmetry under a bias voltage. We observed that the symmetric quantum metric is related to LPGE, whereas the antisymmetric Berry curvature is related to CPGE. The generation rate of the carrier is determined via the integral of the quantum metric in the partial domain of momentum space where the resonance condition is satisfied. Our study established close connections between the nonlinear optical response of the system using TRIS and the QGT of quantum states. Further, it provides a new interpretation for the nonlinear optical response in the view of the tensor field and facilitates the detection of the QGT via photocurrent measurement.

This work was supported by the National Natural Science Foundation of China (Grant No. 11604068). Yu Gu is supported by the National Key R&D Program of China (Grant No. 2017YFA0305500), and Natural Science Foundation of Jiangsu Province (Grant No. BK20200071). Toshiaki Iitaka is supported by MEXT via "Exploratory Challenge on Post-K Computer" (Frontiers of Basic Science: Challenging the Limits).

Supporting Information

The supporting information is available online at phys.scichina.com and link.springer.com. The supporting materials are published as submitted, without typesetting or editing. The responsibility for scientific accuracy and content remains entirely with the authors.

1 D. Xiao, M. C. Chang, and Q. Niu, Rev. Mod. Phys. **82**, 1959 (2010), arXiv: 0907.2021.
2 M. Kolodrubetz, D. Sels, P. Mehta, and A. Polkovnikov, Phys. Rep. **697**, 1 (2017), arXiv: 1602.01062.
3 R. Resta, Rev. Mod. Phys. **66**, 899 (1994).
4 R. Resta, and D. Vanderbilt, *Physics of Ferroelectrics*, edited by C. H. Ahn, K. M. Rabe, and J. M. Triscone (Springer-Verlag, Heidelberg, 2007), Vol. 105, pp. 31-68.
5 J. P. Provost, and G. Vallee, Commun. Math. Phys. **76**, 289 (1980).
6 M. Berry, *Geometric Phases in Physics*, edited by F. Wilczek, and A. Shapere (World Scientific, Singapore, 1989), pp. 7-28.
7 Y. Q. Ma, S. Chen, H. Fan, and W. M. Liu, Phys. Rev. B **81**, 245129 (2010), arXiv: 1003.4040.
8 R. Resta, Eur. Phys. J. B **79**, 121 (2011).
9 T. Holder, D. Kaplan, and B. Yan, Phys. Rev. Res. **29**, 033100 (2020).
10 M. Z. Hasan, and C. L. Kane, Rev. Mod. Phys. **82**, 3045 (2010), arXiv: 1002.3895.
11 X. L. Qi, and S. C. Zhang, Rev. Mod. Phys. **83**, 1057 (2011), arXiv: 1008.2026.
12 Y. Ando, J. Phys. Soc. Jpn. **82**, 102001 (2013), arXiv: 1304.5693.
13 F. D. M. Haldane, Rev. Mod. Phys. **89**, 040502 (2017).
14 B. Bradlyn, J. Cano, Z. Wang, M. G. Vergniory, C. Felser, R. J. Cava, and B. A. Bernevig, Science **353**, aaf5037 (2016).
15 H. Weng, C. Fang, Z. Fang, and X. Dai, Phys. Rev. B **94**, 165201 (2016), arXiv: 1605.05186.
16 N. P. Armitage, E. J. Mele, and A. Vishwanath, Rev. Mod. Phys. **90**, 015001 (2018), arXiv: 1705.01111.
17 Y. Gao, S. A. Yang, and Q. Niu, Phys. Rev. Lett. **112**, 166601 (2014), arXiv: 1402.2538.
18 A. Srivastava, and A. Imamoğlu, Phys. Rev. Lett. **115**, 166802 (2015), arXiv: 1507.04040.
19 A. Gianfrate, O. Bleu, L. Dominici, V. Ardizzone, M. De Giorgi, D. Ballarini, G. Lerario, K. W. West, L. N. Pfeiffer, D. D. Solnyshkov, D. Sanvitto, and G. Malpuech, Nature **578**, 381 (2020).
20 J. E. Sipe, and A. I. Shkrebtii, Phys. Rev. B **61**, 5337 (2000).
21 R. W. Boyd, *Nonlinear Optics* (3rd ed.) (Elsevier, New York, 2008).
22 Y. R. Shen, Nature **337**, 519 (1989).
23 E. Deyo, L. E. Golub, E. L. Ivchenko, and B. Spivak, arXiv: 0904.1917.
24 T. Morimoto, and N. Nagaosa, Sci. Adv. **2**, e1501524 (2016), arXiv: 1510.08112.
25 E. J. König, H. Y. Xie, D. A. Pesin, and A. Levchenko, Phys. Rev. B **96**, 075123 (2017), arXiv: 1705.03903.

26 D. E. Parker, T. Morimoto, J. Orenstein, and J. E. Moore, Phys. Rev. B **99**, 045121 (2019), arXiv: 1807.09285.
27 F. Hipolito, T. G. Pedersen, and V. M. Pereira, Phys. Rev. B **94**, 045434 (2016), arXiv: 1605.04918.
28 A. Taghizadeh, F. Hipolito, and T. G. Pedersen, Phys. Rev. B **96**, 195413 (2017), arXiv: 1710.01300.
29 P. Hosur, Phys. Rev. B **83**, 035309 (2011), arXiv: 1006.5046.
30 D. Rees, K. Manna, B. Lu, T. Morimoto, H. Borrmann, C. Felser, J. E. Moore, D. H. Torchinsky, and J. Orenstein, Sci. Adv. **6**, eaba0509 (2020).
31 F. de Juan, A. G. Grushin, T. Morimoto, and J. E. Moore, Nat. Commun. **8**, 15995 (2017), arXiv: 1611.05887.
32 H. Rostami, and M. Polini, Phys. Rev. B **97**, 195151 (2018), arXiv: 1705.09915.
33 J. Ahn, G.-Y. Guo, and N. Nagaosa, Phys. Rev. X **10**, 041041 (2020).
34 Z. Ni, K. Wang, Y. Zhang, O. Pozo, B. Xu, X. Han, K. Manna, J. Paglione, C. Felser, A. G. Grushin, F. de Juan, E. J. Mele, and L. Wu, Nat. Commun. **12**, 154 (2021).
35 Z. Ni, B. Xu, M. Sánchez-Martínez, Y. Zhang, K. Manna, C. Bernhard, J. W. F. Venderbos, F. de Juan, C. Felser, A. G. Grushin, and L. Wu, npj Quantum Mater. **5**, 96 (2020), arXiv: 2005.13473.
36 I. Sodemann, and L. Fu, Phys. Rev. Lett. **115**, 216806 (2015), arXiv: 1508.00571.
37 D. Culcer, A. Sekine, and A. H. MacDonald, Phys. Rev. B **96**, 035106 (2017).
38 P. Bhalla, A. H. MacDonald, and D. Culcer, Phys. Rev. Lett. **124**, 087402 (2020), arXiv: 1910.06570.
39 S. Nandy, and I. Sodemann, Phys. Rev. B **100**, 195117 (2019), arXiv: 1901.04467.
40 C. Xiao, Z. Z. Du, and Q. Niu, Phys. Rev. B **100**, 165422 (2019), arXiv: 1907.00577.
41 Y. Zhang, J. van den Brink, C. Felser, and B. Yan, 2D Mater. **5**, 044001 (2018).
42 Z. Z. Du, C. M. Wang, H. Z. Lu, and X. C. Xie, Phys. Rev. Lett. **121**, 266601 (2018), arXiv: 1812.10357.
43 Z. Z. Du, C. M. Wang, S. Li, H. Z. Lu, and X. C. Xie, Nat. Commun. **10**, 3047 (2019), arXiv: 1812.08377.
44 Q. Ma, S. Y. Xu, H. Shen, D. MacNeill, V. Fatemi, T. R. Chang, A. M. Mier Valdivia, S. Wu, Z. Du, C. H. Hsu, S. Fang, Q. D. Gibson, K. Watanabe, T. Taniguchi, R. J. Cava, E. Kaxiras, H. Z. Lu, H. Lin, L. Fu, N. Gedik, and P. Jarillo-Herrero, Nature **565**, 337 (2019).
45 N. B. Schade, D. I. Schuster, and S. R. Nagel, Proc. Natl. Acad. Sci. USA **116**, 24475 (2019), arXiv: 1902.03445.
46 K. S. Virk, and J. E. Sipe, Phys. Rev. B **76**, 035213 (2007).
47 D. J. Passos, G. B. Ventura, J. M. V. P. Lopes, J. M. B. L. Santos, and N. M. R. Peres, Phys. Rev. B **97**, 235446 (2018), arXiv: 1712.04924.
48 J. Rammer, and H. Smith, Rev. Mod. Phys. **58**, 323 (1986).
49 W. K. Tse, and A. H. MacDonald, Phys. Rev. Lett. **105**, 057401 (2010), arXiv: 1003.2260.
50 Z. Li, Y. Q. Jin, T. Tohyama, T. Iitaka, J. X. Zhang, and H. Su, Phys. Rev. B **97**, 085201 (2018).
51 Z. Li, A. Tudi, P. Ren, Y. Yang, T. Iitaka, T. Tohyama, Z. Yang, S. Pan, and H. Su, Phys. Rev. Mater. **3**, 025201 (2019).
52 E. I. Blount, *Solid State Physics: Advances in Research and Applications* (Academic, New York, 1962), Vol. 13.
53 M. M. Vazifeh, and M. Franz, Phys. Rev. Lett. **111**, 027201 (2013), arXiv: 1303.5784.
54 M. A. Becker, R. Vaxenburg, G. Nedelcu, P. C. Sercel, A. Shabaev, M. J. Mehl, J. G. Michopoulos, S. G. Lambrakos, N. Bernstein, J. L. Lyons, T. Stöferle, R. F. Mahrt, M. V. Kovalenko, D. J. Norris, G. Rainó, and A. L. Efros, Nature **553**, 189 (2018), arXiv: 1707.03071.
55 M. E. Madjet, G. R. Berdiyorov, F. El-Mellouhi, F. H. Alharbi, A. V. Akimov, and S. Kais, J. Phys. Chem. Lett. **8**, 4439 (2017).
56 D. Niesner, M. Hauck, S. Shrestha, I. Levchuk, G. J. Matt, A. Osvet, M. Batentschuk, C. Brabec, H. B. Weber, and T. Fauster, Proc. Natl. Acad. Sci. USA **115**, 9509 (2018).
57 Y. Zhou, Y. Huang, X. Xu, Z. Fan, J. B. Khurgin, and Q. Xiong, Appl. Phys. Rev. **7**, 041313 (2020).
58 C. Guo, Y. Hu, G. Chen, D. Wei, L. Zhang, Z. Chen, W. Guo, H. Xu, C. N. Kuo, C. S. Lue, X. Bo, X. Wan, L. Wang, A. Politano, X. Chen, and W. Lu, Sci. Adv. **6**, eabb6500 (2020).